

Numerical simulations of Darcy –Forchheimer flow explored with carbon nanotubes under activation energy

 OPEN ACCESS

Received: 31.03.2021

Accepted: 19.05.2021

Published: 05.06.2021

P S S Nagalakshmi^{1*}, N Vijaya¹

¹ Department of Mathematics, Koneru Lakshmaiah Education Foundation, Deemed to be University, Vaddeswaram, Guntur, 522502, Andhra Pradesh, India

Abstract

Citation: Nagalakshmi PSS, Vijaya N (2021) Numerical simulations of Darcy –Forchheimer flow explored with carbon nanotubes under activation energy. Indian Journal of Science and Technology 14(20): 1661-1676. <https://doi.org/10.17485/IJST/v14i20.544>

* Corresponding author.

sathya.krishnat@gmail.com

Funding: None

Competing Interests: None

Copyright: © 2021 Nagalakshmi & Vijaya. This is an open access article distributed under the terms of the [Creative Commons Attribution License](#), which permits unrestricted use, distribution, and reproduction in any medium, provided the original author and source are credited.

Published By Indian Society for Education and Environment ([iSee](#))

ISSN

Print: 0974-6846

Electronic: 0974-5645

Objectives: To obtain the results of the computational analysis of three-dimensional Darcy-Forchheimer flow concerning the hall current and Joule heating with Arrhenius activation energy explored using single-wall carbon nanotube and multi-wall carbon nanotube. **Methods:** The flow equations are modified to a nonlinear system of ordinary differential equations with adequate self-similarity functions. The solution to the modified system is evaluated by numerical techniques with python coding. **Findings:** In this study, the outcomes of engineering parameters are evaluated numerically. Influence of governing parameters on momentum, thermal, and concentration boundary layers are depicted graphically with different base fluids explored with single and multi-wall carbon nanotubes under Darcy -Forchheimer flow of nanofluid. **Novelty:** A favorable comparison is performed with previously available outcomes. The achieved results are almost like solutions obtained by other researchers. Carbon nanotubes are additionally used in an incredible range of applications in electronic, structural engineering, biomedical, energy management, and chemical processing.

Keywords: Activation energy; hall current with ion slip; joule heating; carbon nanotube; python

1 Introduction

Carbon Nanotubes are the only atomically thick tubes formed by a graphite layer enclosing hexagonal carbon atoms. The folding direction of the graphite foil is determined by the chiral vector $Ch(n, m)$, so CNTs can be divided into chiral nanotubes (n, m) , zigzag nanotubes $(n, 0)$, and chair nanotubes (n, n) . Carbon nanotubes have become one of the most studied materials in the past decade due to their promising mechanical, electrical, and thermal properties. Single wall nanotubes (SWCNT) contain a cylinder, while multilayer nanotubes (MWCNT) have multiple concentric cylinders separated by almost equal distances because van der Wall's graphite plates are stacked on top of each other.

Nanofluid is an innovative type of resolution, which is provided by dispersing nanoscale materials (nanoparticles, nanofibers, nanotubes, nanowires, nanorods, nanofilters or droplets) in a base fluid. Creep associated with nanofluids is used

in biomedicine, that is, in radiotherapy of cancer. Choi demonstrated in 1995 that an advanced heat transfer recovery technology uses nano-scale particles in the base fluid. The literature on this subject is very rich. Effect of Joule Heating and Thermal Radiation in Flow of Third Grade Fluid over Radiative Surface obtained by Hayat et al.⁽¹⁾. Similarity solution to three-dimensional boundary layer flow of second grade nanofluid past a stretching surface with thermal radiation and heat source/sink solved by Hayat et al.⁽²⁾. Sreenivasulu and Reddy⁽³⁾ presented the lie group analysis for boundary layer flow of nanofluids near the stagnation-point over a permeable stretching surface embedded in a porous medium in the presence of radiation and heat generation/absorption. Influence of viscous dissipation and Joule heating on MHD bio-convection flow over a porous wedge in the presence of nanoparticles and gyrotactic microorganisms has been explored by Khan et al.⁽⁴⁾. Afshar et al⁽⁵⁾ considered the effect of dispersed nanoparticles on thermophysical properties of nanofluid and heat transfer coefficients. Influence of joule heating and non-linear radiation on MHD 3D dissipating Flow of casson nanofluid past a non-linear stretching sheet has been analyzed by Sreenivasulu et al.⁽⁶⁾. Shahzada et al.⁽⁷⁾ studied the numerical simulation of magnetohydrodynamic Jeffrey nanofluid flow and heat transfer over a stretching sheet considering joule heating and viscous dissipation. Simultaneous impacts of joule heating and variable heat source/sink on MHD 3D flow of carreau-nano liquids with temperature dependent viscosity has been solved by Ramana Reddy et al.⁽⁸⁾. Gholinia et al.⁽⁹⁾ obtained the results of investigation on ethylene glycol nanofluid flow over a vertical permeable circular cylinder under effect of magnetic field. Jodh Singh et al.⁽¹⁰⁾ described the heat transfer using nanofluid. Effect of Joule heating on the flow over an exponentially stretching sheet with convective thermal condition has been conferred by Srinivasacharya et al.⁽¹¹⁾. Magneto hydrodynamic AA7072-AA7075/methanol hybrid nanofluid flow above an uneven thickness surface with slip effect has been propounded by Iskanderet al.⁽¹²⁾. In 1856, Henry Darcy forced the pioneers to add a homogeneous liquid to the flow through the porous medium. However, the classic Darcy's law does not apply to flows with huge velocity and high permeability. To overcome this shortcoming, Forchheimer subsequently modified the Darcian velocity expression by adding the square of the velocity to the moment equation to estimate the collision velocity in the moment equation, and to evaluate the influence of inertia and the flux of physical phenomena. The term "Forchheimer" was first coined by Muscat and is usually used for huge Reynolds numbers, because the filtration rate is actually very high and it creates secondary resistance to the porous medium in the bending moment equation. Importance of Darcy–Forchheimer porous medium in 3D convective flow of carbon nanotubes shown by Alzahrani⁽¹³⁾. Numerical study of Darcy–Forchheimer model with activation energy subject to chemically reactive species and momentum slip of order two analyzed by Majeed et.al⁽¹⁴⁾. A revised model for Darcy–Forchheimer three-dimensional flow of nanofluid subject to convective boundary condition explained by Muhammad et.al⁽¹⁵⁾. Darcy–Forchheimer flow of hydromagnetic nanofluid over a stretching/shrinking sheet in a thermally stratified porous medium with second order slip, viscous and Ohmic dissipations effects results obtained by Vishnu Ganesh et.al⁽¹⁶⁾. Hosseinzadeh et.al⁽¹⁷⁾ investigated on cross-fluid flow containing motile gyrotactic microorganisms and nanoparticles over a three-dimensional cylinder. Hosseinzadeh et.al⁽¹⁸⁾ studied on entropy generation of three-dimensional Bödewadt flow of water and hexanol base fluid suspended by Fe₃O₄ and MoS₂ hybrid nanoparticles.

Investigators scrutinized the onset of binary chemical reaction with an activation energy, joule heating and hall current with ion slip in Darcy–Forchheimer flow of carbon nanotubes over a variable thickness of stretched surface through python. Python with the BVP has been established for the solutions of ODEs. The graphical portrayal is depicted and tables are structured with elaborated. Researchers found that this is the first study using python code as compared to related literature.

2 Materials and Methods

We scrutinize steady 3D magnetohydrodynamic (MHD) convective Darcy –Forchheimer flow explored with carbon nanotubes over a variable thickness of stretched under the influence of Joule heating, hall current with ion slip, and Arrhenius activation energy. Here the fluid is electrically conducting in the presence of applied magnetics $\vec{B} = (\mathbf{0}, \mathbf{0}, B_0)$ and electric $\vec{E} = (\mathbf{0}, -E_0, \mathbf{0})$ field. The flow is induced by a stretching Surface in two nearby x and y directions with velocity p, q respectively. The electric and magnetic fields were carried out through Ohm's law. The induced magnetic flux and Hall current effects are ignored subject to small magnetic Reynolds numbers. Both the electrical and magnetic fields contribute to the momentum and thermal boundary layer equations. Furthermore, the concentration equation deals with the impact of Arrhenius energy of activation with binary reaction. In this clarification, the Brownian and thermophoresis nanoparticles are also engaged. The relevant equations in the afforested conditions can be expressed as follows (14):

$$\frac{\partial p}{\partial x} + \frac{\partial q}{\partial y} + \frac{\partial r}{\partial z} = 0 \quad (1)$$

$$\left(p \frac{\partial p}{\partial x} + q \frac{\partial p}{\partial y} + r \frac{\partial p}{\partial z} - 2\Omega q \right) \rho_{nf} = \mu_{nf} \frac{\partial^2 p}{\partial z^2} - \sigma_{nf} B_0^2 \frac{(qme - pne)}{me^2 + ne^2} - \frac{\mu_{nf}}{k^*} p - \frac{c_f \rho_{nf}}{\sqrt{k^*}} p^2 + \sigma_{nf} E_0 B_0 \quad (2)$$

$$\left(p \frac{\partial q}{\partial x} + q \frac{\partial q}{\partial y} + r \frac{\partial q}{\partial z} - 2\Omega p \right) \rho_{nf} = \mu_{nf} \frac{\partial^2 q}{\partial z^2} - \sigma_{nf} B_0^2 \frac{(qme - pne)}{me^2 + ne^2} - \frac{\mu_{nf}}{k^*} q - \frac{c_f \rho_{nf}}{\sqrt{k^*}} q^2 + \sigma_{nf} E_0 B_0 \quad (3)$$

$$\left(p \frac{\partial T}{\partial x} + q \frac{\partial T}{\partial y} + r \frac{\partial T}{\partial z} \right) (\rho c_p)_{nf} = K_{nf} \frac{\partial^2 T}{\partial z^2} - \frac{\partial q_r}{\partial z} + \mu_{nf} \frac{\partial p}{\partial z} + \sigma_{nf} \left(\frac{(p+q)}{me^2 + ne^2} B_0 - E_0 \right)^2 \quad (4)$$

$$\left(p \frac{\partial C}{\partial x} + q \frac{\partial C}{\partial y} + r \frac{\partial C}{\partial z} \right) = D_B \frac{\partial^2 C}{\partial z^2} - k_r^2 (C - C_\infty) \left(\frac{T}{T_\infty} \right)^n \exp \left(\frac{-E^*}{kT} \right) + \frac{D_T}{T_\infty} \frac{\partial^2 T}{\partial z^2} \quad (5)$$

Subject to the boundary conditions at $z \rightarrow 0$

$$\begin{aligned} p &= p_1 \left(\exp \left(\frac{x+y+c}{L} \right) \right)^m, q = q_1 \left(\exp \left(\frac{x+y+c}{L} \right) \right)^m, r = 0 \\ -K_{nf} \frac{\partial T}{\partial z} &= -h_f (T_w - T), \frac{\partial C}{\partial z} = -h_m (C_w - C) \end{aligned} \quad (6)$$

Subject to the boundary conditions at $z \rightarrow \infty$

$$p = q = 0, T = T_\infty, C = C_\infty \quad (7)$$

Here p , q , and r are the velocity components in x , y , and z directions respectively μ_{nf} dynamic nanofluid viscosity, $m_e = 1 + n_i n_e$, where n_i is denoted the ion-slip while n_e is the hall current parameters, ρ_{nf} density of nanofluid, K_{nf} thermal conductivity of nanofluid, σ_{nf} electrical conductivity of nanofluid, c_f inertia resistance force, k^* permeability of porous medium, c_p specific heat, D_B , D_T Brownian and thermal diffusion coefficient, h_f , h_m the wall heat and wall mass transport coefficients. Moreover, n is the fitted rate constant ($-1 < n < 1$), k_r the reaction rate, E^* the activation energy, k the Boltzmann constant, whole expression $k_r^2 \left(\frac{T}{T_\infty} \right)^n \exp \left(\frac{-E^*}{kT} \right)$ entitled as modified Arrhenius equation. For thermal radiation we utilize the Rossel estimation, and then the radiative heat flux is defined as

$$q_r = \frac{-16\sigma^* T_\infty^3}{k^s} \frac{\partial T}{\partial z} \quad (8)$$

Here σ^* , k^s are the Stefan-Boltzmann constant and mean absorption coefficient, respectively.

Nanofluid parameters:

$$\nu_{nf} = \frac{\mu_{nf}}{\rho_{nf}}, \mu_{nf} = \frac{\mu_{bf}}{(1-\varphi)^{2.5}}, \rho_{nf} = (1-\varphi) \rho_{bf} + \varphi \rho_{CNT}, (\rho c_p)_{nf} = (1-\varphi) (\rho c_p)_{bf} + \varphi (\rho c_p)_{CNT}$$

$$\frac{K_{nf}}{K_{bf}} = \frac{(1-\varphi)(K_{CNT} - K_{bf}) + 2\varphi K_{CNT} \ln \left(\frac{K_{CNT} + K_{bf}}{2K_{bf}} \right)}{(1-\varphi)(K_{CNT} - K_{bf}) + 2\varphi K_{bf} \ln \left(\frac{K_{CNT} + K_{bf}}{2K_{bf}} \right)}, \frac{\sigma_{nf}}{\sigma_{bf}} = 1 + \frac{3(\sigma_{CNT} - \sigma_{bf})\varphi}{(\sigma_{CNT} + 2\sigma_{bf}) - (\sigma_{CNT} - \sigma_{bf})\varphi} \quad (9)$$

Suitable conversions:

Let us consider

$$\begin{aligned} p &= P f'(\eta), q = P g'(\eta), r = - \left(\frac{mv_{bf} P}{2L} \right)^{0.5} ((f+g) + \eta (f' + g')) \\ \theta(\eta) &= \frac{T - T_\infty}{T_w - T_\infty}, h(\eta) = \frac{c - C_\infty}{C_w - C_\infty}, P = p_1 \left(\exp \left(\frac{x+y+c}{L} \right) \right)^m, \eta = \left(\frac{mP}{2v_{bf} L} \right)^{0.5} z \end{aligned} \quad (10)$$

Here p_1 , c , and m are constants and L is the reference distance.

The above transformations satisfy Eq. (1) automatically and Eqs. (2)–(5) with Eqs. (6) and (7) reduce to the following ODEs

$$\begin{aligned} A_2 f''' - K_1(M1)A_5 \frac{(m\epsilon g' - n\epsilon f')}{m\epsilon^2 + n\epsilon^2} - \frac{A_2 K_1}{P_0} f' - (Fi)K_1 A_1 (f')^2 \\ + (M1)(E1)K_1 A_5 - A_1 \left(2(f')^2 + 2g'f' - f''f - f''g - 2\epsilon g' \right) = 0 \end{aligned} \quad (11)$$

$$\begin{aligned} A_2 g''' - K_1(M1)A_5 \frac{m\epsilon g' - n\epsilon f'}{m\epsilon^2 + n\epsilon^2} - \frac{A_2 K_1}{P_0} g' - (Fi)K_1 A_1 (g')^2 \\ + (M1)(E1)K_1 A_5 - A_1 \left(2(g')^2 + 2g'f' - g''g - g''f - 2\epsilon f' \right) = 0 \end{aligned} \quad (12)$$

$$\begin{aligned} A_4 \left(\left(1 + \frac{4}{3} \frac{R}{A_4} \right) \theta'' + \frac{(M1)K_1(\text{Pr})(Ec)A_5}{A_4} \left(\frac{f' + g'}{m\epsilon^2 + n\epsilon^2} - (E1) \right)^2 + \frac{A_1}{A_4} (\text{Pr})(Ec) (f'')^2 \right) \\ - (\text{Pr})A_3 (2f'\theta + 2g'\theta - \theta'f - \theta'g) = 0 \end{aligned} \quad (13)$$

$$\begin{aligned} \left(h'' + \frac{Nt}{Nb} \theta'' \right) - K_1(\text{Pr})(Le)(\delta 2)h(1 + (\delta 1)\theta)^m \exp \left(\frac{-E}{1 + \delta_1 \theta} \right) \\ - Sc \left(2hf' + 2hg' - fh' - gh' \right) = 0 \end{aligned} \quad (14)$$

$$\begin{aligned} f(0) = 0, g(0) = 0, f'(0) = 1, g'(0) = \beta \\ \theta'(0) = - \left(\frac{2}{m} \right)^{0.5} \left(\frac{1}{A_4} \right) \gamma_T (1 - \theta(0)), h'(0) = - \left(\frac{2}{m} \right)^{0.5} \gamma_C (1 - h(0)), \\ f'(\infty) = 0, g'(\infty) = 0, \theta(\infty) = 0, h(\infty) = 0 \end{aligned} \quad (15)$$

Dimensionless parameters:

$$\begin{aligned} A_1 = (1 - \varphi) + \varphi \frac{\rho_{\text{CNT}}}{\rho_{\text{bf}}}, \quad A_2 = \frac{1}{(1 - \varphi)^{2.5}}, \quad A_3 = (1 - \varphi) + \varphi \frac{(\rho c_p)_{\text{CNT}}}{(\rho c_p)_{\text{bf}}} \\ A_4 = \frac{(1 - \varphi)(K_{\text{CNT}} - K_{\text{bf}}) + 2\varphi K_{\text{CNT}} \ln \left(\frac{K_{\text{CNT}} + K_{\text{bf}}}{2K_{\text{bf}}} \right)}{(1 - \varphi)(K_{\text{CNT}} - K_{\text{bf}}) + 2\varphi K_{\text{bf}} \ln \left(\frac{K_{\text{CNT}} + K_{\text{bf}}}{2K_{\text{bf}}} \right)}, \quad A_5 = 1 + \frac{3(\sigma_{\text{CNT}} - \sigma_{\text{bf}})\varphi}{(\sigma_{\text{CNT}} + 2\sigma_{\text{bf}}) - (\sigma_{\text{CNT}} - \sigma_{\text{bf}})\varphi} \\ K_1 = \frac{1}{m}, \quad \beta = \frac{q_1}{p_1}, \quad M1 = \frac{2\sigma_{\text{bf}}B_0^2L}{\rho_{\text{bf}}P}, \quad E1 = \frac{E_0}{PB_0}, \quad Po = \frac{Pk^*}{2V_{\text{bf}}L}, \quad Fi = \frac{2c_f L}{\sqrt{k^*}}, \quad R = \frac{4\sigma^* T_\infty^3}{k^* k_{\text{bf}}}, \quad \epsilon = \frac{2L\Omega}{P} \\ \gamma_T = \frac{h_f}{K_{\text{bf}}} \left(\frac{V_{\text{bf}}L}{P} \right)^{0.5}, \quad \gamma_C = \frac{h_f}{D_B} \left(\frac{V_{\text{bf}}L}{P} \right)^{0.5}, \quad \text{Pr} = \frac{(\rho c_p)_{\text{bf}} V_{\text{bf}}}{k}, \quad Ec = \frac{P^2}{(c_p)_{\text{bf}} \Delta T}, \quad Sc = \frac{V_{\text{bf}}}{D_B} \\ Nt = \frac{(\rho c_p)_{\text{CNT}} D_T \Delta T}{V_{\text{bf}} T_\infty (\rho c_p)_{\text{bf}}}, \quad Nb = \frac{(\rho c_p)_{\text{CNT}} D_B \Delta C}{V_{\text{bf}} (\rho c_p)_{\text{bf}}}, \quad E = \frac{E^*}{kT_\infty}, \quad \delta 1 = \frac{\Delta T}{T_\infty}, \quad \delta 2 = \frac{2k_r^2 L}{P}. \end{aligned} \quad (16)$$

Engineering parameters

Engineering parameters like skin friction coefficient C_{fx} , C_{fy} , local Nusselt Nu_x , and Sherwood Sh_x numbers are defined as

$$C_{fx} = \frac{\tau_{wx}}{\rho_{\text{bf}} P^2}, \quad C_{fy} = \frac{\tau_{wy}}{\rho_{\text{bf}} P^2}, \quad Nu_x = \frac{x q_w}{K_{\text{bf}} \Delta T}, \quad Sh_x = \frac{x J_w}{D_B \Delta C}. \quad (17)$$

in which τ_w , q_w , and J_w denote the surface shear stress, the surface heat flux and the surface mass flux respectively. Here

$$\tau_{wx} = \mu_{nf} \left(\frac{\partial p}{\partial z} \right)_{z=0}, \quad \tau_{wy} = \mu_{nf} \left(\frac{\partial q}{\partial z} \right)_{z=0}, \quad q_w = -K_{nf} \left(\frac{\partial T}{\partial z} \right)_{z=0}, \quad J_w = -D_B \left(\frac{\partial C}{\partial z} \right)_{z=0}. \quad (18)$$

Therefore, the dimensionless forms of overhead quantities are

$$\begin{aligned} (\text{Re}_x)^{0.5} C_{fx} &= \left(\frac{m}{2} \right)^{0.5} \frac{1}{(1-\varphi)^{2.5}} f''(0), \quad (\text{Re}_x)^{0.5} C_{fy} = \left(\frac{m}{2} \right)^{0.5} \frac{1}{(1-\varphi)^{2.5}} g''(0), \\ (\text{Re}_x)^{0.5} \text{Nu}_x &= - \left(\frac{m}{2} \right)^{0.5} \left(\frac{(1-\varphi)(K_{CNT} - K_{bf}) + 2\varphi K_{CNT} \ln \left(\frac{K_{CNT} + K_{bf}}{2K_{bf}} \right)}{(1-\varphi)(K_{CNT} - K_{bf}) + 2\varphi K_{bf} \ln \left(\frac{K_{CNT} + K_{bf}}{2K_{bf}} \right)} \right) \theta'(0), \\ (\text{Re}_x)^{0.5} Sh_x &= - \left(\frac{m}{2} \right)^{0.5} h'(0), \end{aligned} \quad (19)$$

in which $\text{Re}_x = \frac{xP}{V_{bf}}$ is the local Reynolds number.

3 Results and discussion

To attain this, the BVP scheme is engaged to discretize the governing equations into a well-ordered problem. For this determination, researchers revise equations (11)-(15) into first-order differential systems. Thus, in the present study, the value of $\eta = \eta_{\max}$ is taken to be 10, and step-size is taken to be $\Delta \eta = 0.01$ with a relative error tolerance of 10^{-5} . The relative study of present results with those obtained by Hayat et.al⁽¹⁾ is shown in Tables 1, 2 and 3. When compared to the other method obtained by Hayat et.al⁽¹⁾ while equating the parameters of momentum, thermal, and concentration to zero for getting accuracy through python code.

Table 1. Accuracy assessment of $f^{11}(0)$, when $m=2$, and remaining parameters of momentum-thermo-physical and concentration are equated to zero

B	Hayat et.al ⁽²⁾	Present
0.0	1.28180856	1.281831634409684
0.5	1.56988846	1.569704938336608
1.0	1.81275105	1.812759680612502

Table 2. Accuracy assessment of $g^{11}(0)$, when $m=2$, and remaining parameters of momentum-thermo-physical and concentration are equated to zero.

B	Hayat et.al ⁽²⁾	Present
0.0	0	0
0.5	0.78494423	0.7848524691689054
1.0	1.81275105	1.8127596806113822

Table 3. Accuracy assessment of $\theta^1(0)$, when $m=2$, $\text{Pr}=0.7$ and remaining parameters of momentum-thermo-physical and concentration are equated to zero.

B	Hayat et.al ⁽²⁾	Present
0.0	-0.42589	-0.44050
0.25	-0.47616	-0.485435
0.50	-0.52161	-0.526539
0.75	-0.56339	-0.564776
1.0	-0.60228	-0.599231

The framework of this study is to scrutinize the properties of Arrhenius activation energy, Joule heating, and hall current with ion-slip with binary chemical reaction on steady 3D magnetohydrodynamic (MHD) convective Darcy –Forchheimer flow explored with carbon nanotubes over a variable thickness of the stretched sheet. Python with a BVP scheme has been executed to elucidate the present ODEs. The boundary layers of numerous parameters on momentum, thermal, and concentration is portrayed and discussed.

Execution of Electric parameter(E1) on $f^1(\eta)$, $g^1(\eta)$, $\theta(\eta)$, and $h(\eta)$

To disclose the enactment of the electric parameter(E1) on momentum, thermal and concentration boundary layers are exposed from Figures 1, 2, 3 and 4. Physically, increasing the values of electric parameter boost the momentum boundary layer, thermal boundary layer, but in contrast, results appear in the concentration boundary layer. This causes that higher estimation of electric parameter relates to intensity of electric and magnetic field.

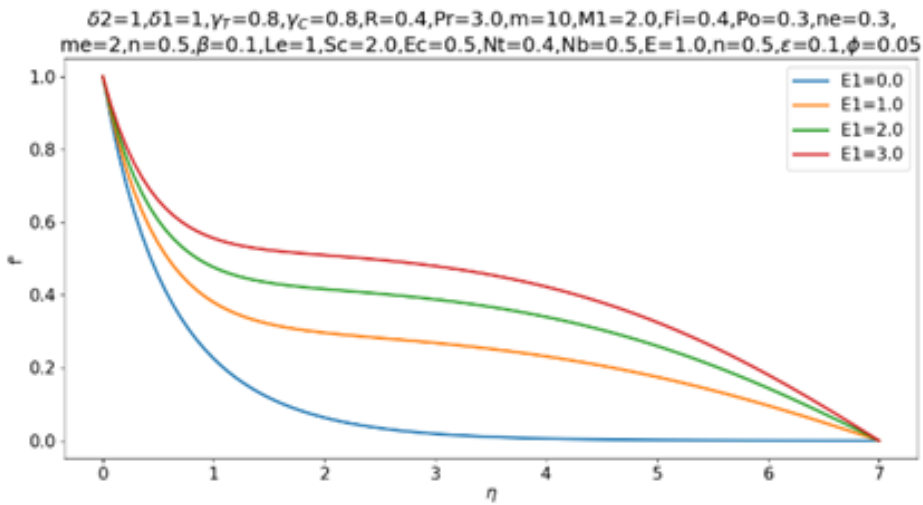


Fig 1. Horizontal velocity [$f^1(\eta)$] via Electric parameter (E1)

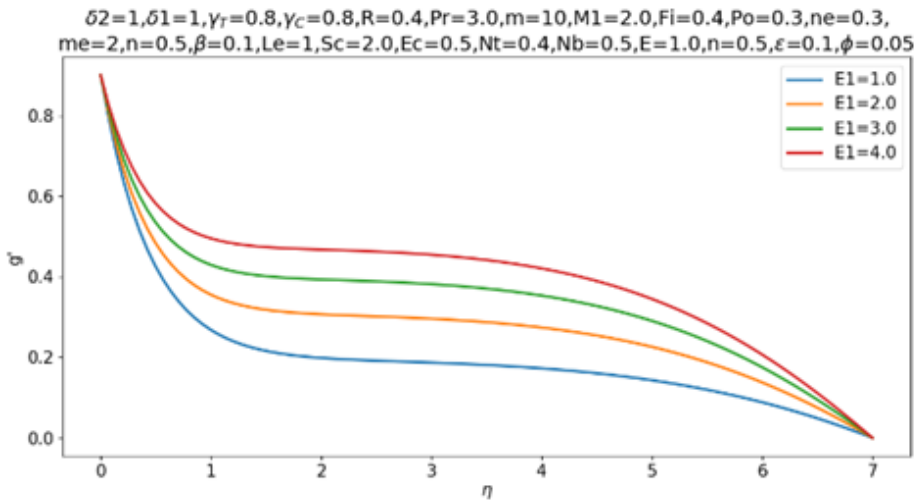
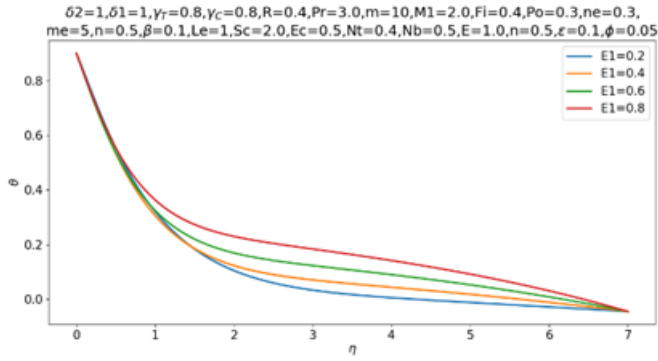
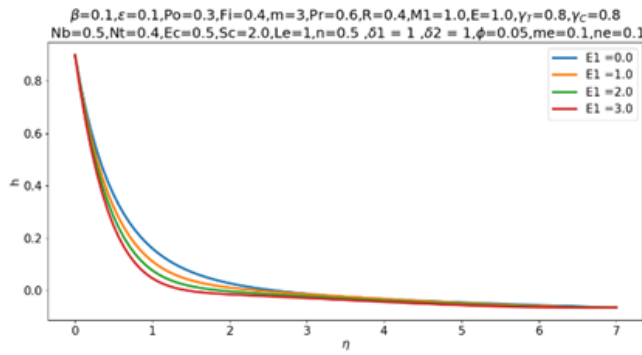
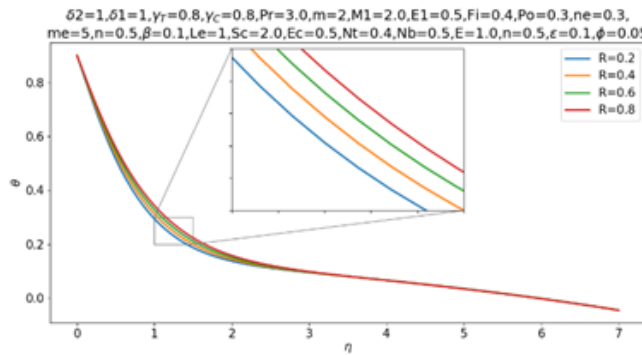


Fig 2. Vertical velocity [$g^1(\eta)$] via Electric parameter (E1)

**Fig 3.** Temperature [$\theta(\eta)$] via Electric parameter (E1)**Fig 4.** Concentration [$h(\eta)$] via Electric parameter (E1)

Execution of radiation parameter (R) on $\theta(\eta)$

Figure 5 scrutinized that intensifying value of R present analogous impact and enhance both the temperature and thermal layer thickness. This causes that higher estimation of radiation relates to the rapid vibration of nanoparticles.

**Fig 5.** Temperature[$\theta(\eta)$] via radiation parameter(R)

Execution of SWCNT and MWCNT on $f^1(\eta)$, $g^1(\eta)$, $\theta(\eta)$, and $h(\eta)$

Figures 6, 7, 8 and 9 Capture the behavior of SWCNT and MWCNT with different base fluids on Momentum, thermal, and concentration boundary layers respectively. The influence of momentum and concentration boundary layers with different base fluids is dominated by MWCNT. The thermal boundary layer is henpecked by SWCNT because of specific heat.

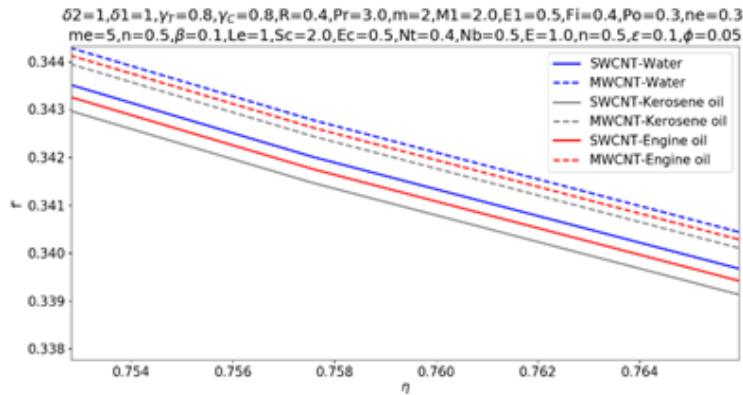


Fig 6. Velocity [$f^1(\eta)$] via SWCNT and MWCNT with different base fluids

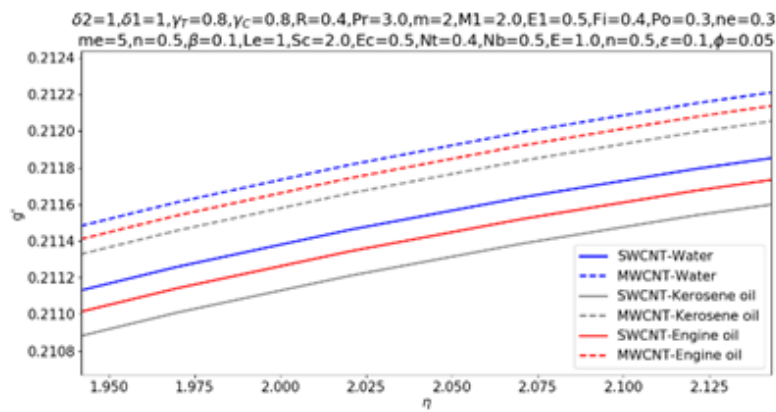


Fig 7. Vertical velocity [$g^1(\eta)$] via SWCNT and MWCNT with different base fluids

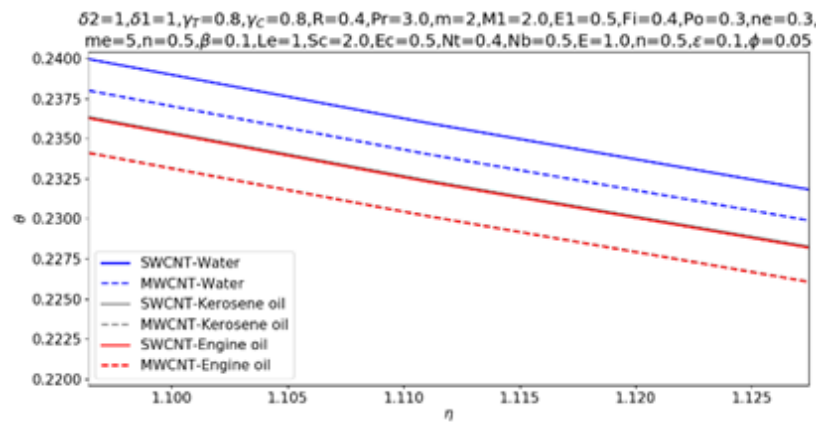
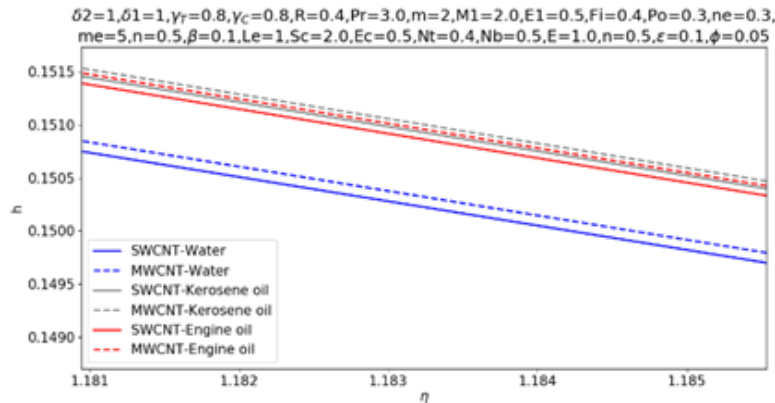


Fig 8. Temperature [$\theta(\eta)$] via SWCNT and MWCNT with different base fluids

**Fig 9.** Concentration [$h(\eta)$] via SWCNT and MWCNT with different base fluids

Tables of local skin friction coefficients, local Nusselt and Sherwood numbers

Behaviors of magnetic parameter(M_1), Electric parameter (E_1), power of exponential stretching sheet parameter(m), rotation parameter(ε), porosity parameter (Po), friction parameter (Fi), nanoparticle volume fraction(ϕ) on skin friction coefficient, local Nusselt number, and local Sherwood number are disclosed in [Tables 4, 5, 6, 7, 8 and 9](#). Investigators interpreted that the skin friction coefficient calibrate for excellent estimations of magnetic parameter, and electric parameter and the local skin friction coefficient crumble with growing power of exponential stretching sheet parameter, porosity parameter, friction parameter, and nanoparticle volume fraction. The local Nusselt and Sherwood numbers boots for magnifying magnetic parameter, Electric parameter, power of exponential stretching sheet parameter, and nanoparticle volume fraction and the local Nusselt and Sherwood numbers wane for higher estimations of rotation parameter, porosity parameter, and friction parameter. Influence of various base fluids explored with multi wall carbon nanotube (MWCNT) on local skin friction coefficient are dominated as compared to single wall carbon nanotube (SWCNT), however contradiction appeared in local Nusselt and Sherwood numbers, due to specific heat of nanoparticles.

Table 4. Coefficients of Skin Friction explored with water-based CNT

	$(Re_x)^{0.5} C_{f_x}$		$(Re_x)^{0.5} C_{f_y}$	
m	SWCNT	MWCNT	SWCNT	MWCNT
1	-0.763489	-0.729187	0.625432	0.635101
2	-1.224687	-1.181661	0.446345	0.455891
3	-1.57556	-1.52556	0.327124	0.336464
4	-1.86877	-1.812759	0.23580	0.244967
5	-2.12531	-2.063925	0.16076	0.169792
ε	SWCNT	MWCNT	SWCNT	MWCNT
0.0	-1.271191	-1.228003	0.539242	0.550536
0.2	-1.182163	-1.139248	0.349305	0.356936
0.3	-1.143789	-1.10093	0.248363	0.253903
0.4	-1.110039	-1.067211	0.143628	0.146883
0.5	-1.081313	-1.038493	0.035255	0.036012
M_1	SWCNT	MWCNT	SWCNT	MWCNT
0.0	-1.6965701	-1.661854	-0.246815	-0.245177
0.2	-1.5836861	-1.546905	-0.064564	-0.061061
0.3	-1.5338970	-1.496195	0.010431	0.014825
0.4	-1.4861684	-1.447600	0.080569	0.085799
0.5	-1.4397164	-1.400314	0.147272	0.153316
E_1	SWCNT	MWCNT	SWCNT	MWCNT
0.0	-1.699203	-1.664444	-0.247223	-0.245606
0.2	-1.593936	-1.557422	-0.063868	-0.060351
0.3	-1.544436	-1.50703	0.010794	0.0151835

Continued on next page

Table 4 continued

0.4	-1.496245	-1.457975	0.080603	0.0858131
0.5	-1.448822	-1.409697	0.147055	0.1530623
Fi	SWCNT	MWCNT	SWCNT	MWCNT
0.0	-1.102136	-1.0615124	0.457235	0.4667986
0.2	-1.164633	-1.1227866	0.451751	0.4613062
0.3	-1.194949	-1.1525079	0.449038	0.4585883
0.4	-1.224687	-1.1816615	0.446345	0.4558919
0.5	-1.253877	-1.2102766	0.443676	0.4532180
Po	SWCNT	MWCNT	SWCNT	MWCNT
0.1	-1.101448	-1.0981814	0.490696	0.4858830
0.2	-1.184205	-1.1402346	0.460712	0.4706713
0.3	-1.224687	-1.1816615	0.446345	0.4558919
0.4	-1.264562	-1.222444	0.432384	0.4415427
0.5	-1.303839	-1.2625935	0.418824	0.4276155
Φ	SWCNT	MWCNT	SWCNT	MWCNT
0.1	-1.049317	-1.3334205	0.4647983	0.4448191
0.2	-1.901082	-1.7158230	0.3777966	0.4129515
0.3	-2.556459	-2.2570260	0.3095976	0.3599152
0.4	-3.514040	-3.0773249	0.2037653	0.2669620
0.5	-5.048507	-4.4423350	0.0224635	0.2669620

Table 5. Coefficients of Local Nusselt and Sherwood numbers explored with water-based CNT

	$(Re_x)^{0.5} Nu_x$		$(Re_x)^{0.5} Sh_x$	
m	SWCNT	MWCNT	SWCNT	MWCNT
1	0.881598	0.869451	1.426537	1.425611
2	1.274521	1.255594	1.898613	1.896743
3	1.545930	1.522809	2.262747	2.260220
4	1.763793	1.737547	2.570623	2.567568
5	1.950197	1.921430	2.84245	2.838948
ε	SWCNT	MWCNT	SWCNT	MWCNT
0.0	1.268236	1.250146	1.906029	1.904407
0.2	1.276328	1.256745	1.890306	1.888183
0.3	1.273219	1.253118	1.880995	1.878606
0.4	1.265198	1.244706	1.870577	1.867905
0.5	1.2518681	1.231095	1.858925	1.855941
M1	SWCNT	MWCNT	SWCNT	MWCNT
0.0	0.9136202	0.907056	1.695696	1.693349
0.2	1.1029004	1.087909	1.761876	1.759531
0.3	1.1428116	1.126658	1.785278	1.782976
0.4	1.1732553	1.156330	1.805731	1.803474
0.5	1.1972706	1.179773	1.824191	1.822008
E1	SWCNT	MWCNT	SWCNT	MWCNT
0.0	0.9143792	0.90787575	1.6955819	1.69324518
0.2	1.1502403	1.13350599	1.7528338	1.75037047
0.3	1.2017732	1.18338601	1.7746351	1.77217257
0.4	1.2377825	1.21838209	1.7944560	1.79201247
0.5	1.2620529	1.24205332	1.8131383	1.8107688
Fi	SWCNT	MWCNT	SWCNT	MWCNT
0.0	1.312747	1.29214719	1.906834	1.904767
0.2	1.293330	1.27358542	1.902595	1.900628
0.3	1.283853	1.26452120	1.900574	1.898655
0.4	1.274521	1.2555948	1.898613	1.896743
0.5	1.265332	1.2468018	1.896709	1.8948875
Po	SWCNT	MWCNT	SWCNT	MWCNT
0.1	1.331488	1.29315858	1.912361	1.90592792

Continued on next page

Table 5 continued

0.2	1.293544	1.27438548	1.903081	1.90127314
0.3	1.274521	1.25559488	1.898613	1.89674334
0.4	1.255474	1.23677044	1.894260	1.89233832
0.5	1.236412	1.21793229	1.890033	1.88807146
Φ	SWCNT	MWCNT	SWCNT	MWCNT
0.1	0.9196978	1.5159484	1.8264048	1.93621604
0.2	1.8894791	1.9030509	1.9686279	1.97719181
0.3	2.1233675	2.1743915	1.9840601	1.99759366
0.4	2.3066253	2.3773794	1.9955089	2.01101773
0.5	2.5062949	2.5588475	2.0084366	2.02321381

Table 6. Coefficients of Skin Friction explored with Kerosene-based CNT

	$(Re_x)^{0.5} C_{f_x}$	$(Re_x)^{0.5} C_{f_y}$		
m	SWCNT	MWCNT	SWCNT	MWCNT
1	-0.78728270	-0.7443184	0.618794252	0.6308222
2	-1.25455768	-1.2006357	0.439783454	0.4516685
3	-1.61029388	-1.5476063	0.320689151	0.3323352
4	-1.90769964	-1.8374533	0.22947459	0.2409181
5	-2.16799310	-2.0909877	0.154521663	0.1658075
ϵ	SWCNT	MWCNT	SWCNT	MWCNT
0.0	-1.30117773	-1.2470478	0.5315067	0.5455338
0.2	-1.21194929	-1.1581743	0.3440288	0.3535671
0.3	-1.17352765	-1.1198359	0.2444878	0.2514672
0.4	-1.13975052	-1.0861030	0.1412802	0.1454674
0.5	-1.11101399	-1.0573839	0.0346131	0.0357135
M1	SWCNT	MWCNT	SWCNT	MWCNT
0.0	-1.7208377	-1.6771385	-0.247993	-0.2458919
0.2	-1.6093339	-1.5631009	-0.067017	-0.0626021
0.3	-1.5601657	-1.5128010	0.007372	0.0128899
0.4	-1.5126781	-1.4645914	0.077107	0.0834923
0.5	-1.4671338	-1.4176768	0.143098	0.1506492
E1	SWCNT	MWCNT	SWCNT	MWCNT
0.0	-1.72348847	-1.6797401	-0.248387	-0.2463107
0.2	-1.61940465	-1.5734994	-0.066330	-0.0618979
0.3	-1.57050528	-1.5235053	0.007737	0.0132498
0.4	-1.52290030	-1.4748334	0.076989	0.0835152
0.5	-1.47605425	-1.4269363	0.142899	0.1504102
Fi	SWCNT	MWCNT	SWCNT	MWCNT
0.0	-1.1303323	-1.0794290	0.4506578	0.4625680
0.2	-1.1936816	-1.1412416	0.4451820	0.4570793
0.3	-1.2244121	-1.1712247	0.4424721	0.4543632
0.4	-1.2545576	-1.2006357	0.4397834	0.4516685
0.5	-1.2841480	-1.2295038	0.4371175	0.4489967
Po	SWCNT	MWCNT	SWCNT	MWCNT
0.1	-1.17430154	-1.1180172	0.4683628	0.4812823
0.2	-1.21470827	-1.1596305	0.4538733	0.4662640
0.3	-1.25455768	-1.2006357	0.4397834	0.4516685
0.4	-1.29382331	-1.2410140	0.4260831	0.4374925
0.5	-1.33251439	-1.2807739	0.4127686	0.4237287
Φ	SWCNT	MWCNT	SWCNT	MWCNT
0.1	-1.48106727	-1.372421	0.413824727	0.4365221
0.2	-2.02385201	-1.799084	0.355116802	0.3969613
0.3	-2.75084994	-2.392287	0.27800306	0.3369254
0.4	-3.79505556	-3.275272	0.16423471	0.2380382
0.5	-5.43889221	-4.717023	-0.02419145	0.0624988

Table 7. Coefficients of Local Nusselt number and Sherwood number explored with Kerosene-based CNT

	$(Re_x)^{0.5} Nu_x$		$(Re_x)^{0.5} Sh_x$	
m	SWCNT	MWCNT	SWCNT	MWCNT
1	0.838838344	0.82985086	1.4151419	1.41365674
2	1.213268473	1.19820199	1.8820387	1.87932240
3	1.47244527	1.45377823	2.2423974	2.23880775
4	1.68077515	1.65950504	2.5471413	2.54284284
5	1.85920227	1.83588313	2.8162258	2.81132052
ϵ	SWCNT	MWCNT	SWCNT	MWCNT
0.0	1.2066017	1.19254704	1.8895487	1.88711932
0.2	1.2156722	1.19979434	1.8736804	1.87066823
0.3	1.2134269	1.19688527	1.8643814	1.86105674
0.4	1.2065505	1.18948258	1.8540344	1.85037131
0.5	1.1947667	1.17720988	1.8425280	1.83848151
M1	SWCNT	MWCNT	SWCNT	MWCNT
0.0	0.8789959	0.8762448	1.6800026	1.67671568
0.2	1.0535758	1.0419437	1.7465854	1.74327940
0.3	1.0904923	1.0777651	1.7698048	1.76655332
0.4	1.1181178	1.1053161	1.7902317	1.78687889
0.5	1.1410841	1.1271501	1.8083639	1.80525805
E1	SWCNT	MWCNT	SWCNT	MWCNT
0.0	0.87958907	0.87690724	1.6799112	1.67664138
0.2	1.098745825	1.08510138	1.7371641	1.73374883
0.3	1.146604947	1.13132109	1.7586978	1.75529094
0.4	1.180061792	1.16381597	1.7782936	1.77491261
0.5	1.202585929	1.18581340	1.7967989	1.79350819
Fi	SWCNT	MWCNT	SWCNT	MWCNT
0.0	1.25027263	1.2333168	1.8897660	1.88684883
0.2	1.23147766	1.2154869	1.8857754	1.88296004
0.3	1.22230241	1.2067787	1.8838771	1.88111161
0.4	1.21326847	1.1982019	1.8820387	1.87932240
0.5	1.20437101	1.1897524	1.8802569	1.87758921
Po	SWCNT	MWCNT	SWCNT	MWCNT
0.1	1.24899191	1.23350801	1.8905160	1.88797419
0.2	1.23114124	1.21586512	1.8862191	1.88358656
0.3	1.21326847	1.19820199	1.8820387	1.87932240
0.4	1.19537341	1.18050540	1.8779686	1.87518054
0.5	1.17746296	1.16279403	1.8740173	1.87116903
Φ	SWCNT	MWCNT	SWCNT	MWCNT
0.1	1.44120937	1.4311677	1.9122720	1.91179294
0.2	1.78364744	1.81440513	1.9423220	1.94872670
0.3	2.03801353	2.12448323	1.9584476	1.96998616
0.4	2.24434980	2.38133492	1.9727971	1.98660227
0.5	2.43371574	2.59387775	1.9902222	2.00364969

Table 8. Coefficients of Skin Friction explored with engine oil-based CNT

	$(Re_x)^{0.5} C_{f_x}$		$(Re_x)^{0.5} C_{f_y}$	
m	SWCNT	MWCNT	SWCNT	MWCNT
1	-1.4076195	-0.7443184	0.42762256	0.6308222
2	-1.6572581	-1.2006357	0.40370852	0.4516685
3	-1.8782380	-1.5476063	0.38235177	0.3323352
4	-2.0783363	-1.8374533	0.36319958	0.2409181
5	-2.2624266	-2.0909877	0.34590040	0.1658075
ϵ	SWCNT	MWCNT	SWCNT	MWCNT
0.0	-1.28529361	-1.2369439	0.5355939	0.5481834

Continued on next page

Table 8 continued

0.2	-1.19617209	-1.1481338	0.3468219	0.3553536
0.3	-1.15777691	-1.1098087	0.2465438	0.2527610
0.4	-1.12401526	-1.0760812	0.1425328	0.1462226
0.5	-1.09528198	-1.0473633	0.0349485	0.0358790
M1	SWCNT	MWCNT	SWCNT	MWCNT
0.0	-1.70797226	-1.6690275	-0.247366	-0.2455113
0.2	-1.59573715	-1.5545037	-0.065716	-0.0617840
0.3	-1.54624188	-1.5039871	0.0089939	0.0139173
0.4	-1.49843913	-1.4555736	0.0790343	0.0847163
0.5	-1.45260471	-1.4084628	0.1453097	0.1520634
E1	SWCNT	MWCNT	SWCNT	MWCNT
0.0	-1.71060950	-1.6716188	-0.247766	-0.2459352
0.2	-1.60590240	-1.5649650	-0.065024	-0.0610765
0.3	-1.55668643	-1.5147617	0.009357	0.0142761
0.4	-1.50877261	-1.4658860	0.078903	0.0847343
0.5	-1.46162259	-1.4177878	0.1450991	0.1518167
Fi	SWCNT	MWCNT	SWCNT	MWCNT
0.0	-1.11539820	-1.0699240	0.454135	0.4648099
0.2	-1.17829564	-1.1314509	0.448655	0.4593192
0.3	-1.20880637	-1.1612949	0.445943	0.4566021
0.4	-1.23873587	-1.1905693	0.443252	0.4539065
0.5	-1.26811386	-1.2193031	0.440585	0.4512337
Po	SWCNT	MWCNT	SWCNT	MWCNT
0.1	-1.15779979	-1.1074957	0.4721304	0.4837195
0.2	-1.19855372	-1.1493414	0.4574886	0.4685991
0.3	-1.23873587	-1.1905693	0.4432529	0.4539065
0.4	-1.27832218	-1.2311616	0.4294155	0.4396389
0.5	-1.31732151	-1.2711269	0.4159714	0.4257888
ϕ	SWCNT	MWCNT	SWCNT	MWCNT
0.1	-1.44950364	-1.3517839	0.4203567675	0.4409025
0.2	-1.95938268	-1.7552095	0.3669605953	0.4053546
0.3	-2.64907930	-2.3212162	0.2944445106	0.3489499
0.4	-3.64813906	-3.1714246	0.1847969512	0.2531525
0.5	-5.23476384	-4.5728929	0.0001387517	0.0800308

Table 9. Coefficients of Local Nusselt number and Sherwood number explored with engine oil based CNT

$(Re_x)^{0.5} Nu_x$	$(Re_x)^{0.5} Sh_x$			
	m	SWCNT	MWCNT	SWCNT
1	1.16679601	0.82985086	1.8735376	1.41365674
2	1.09016705	1.19820199	1.8601454	1.87932240
3	1.02192905	1.45377823	1.8495870	2.23880775
4	0.96021831	1.65950501	1.8410352	2.54284284
5	0.90371873	1.83588313	1.8339723	2.81132052
ε	SWCNT	MWCNT	SWCNT	MWCNT
0.0	1.2115332	1.19496544	1.8910634	1.8881878
0.2	1.2200689	1.20188217	1.8750855	1.8716645
0.3	1.2175664	1.19881388	1.8657164	1.8620066
0.4	1.2104294	1.19124960	1.8552864	1.8512660
0.5	1.1982907	1.17880587	1.8436710	1.8393098
M1	SWCNT	MWCNT	SWCNT	MWCNT
0.0	0.88311093	0.87827153	1.6812307	1.67758681
0.2	1.05749993	1.04381688	1.7477606	1.74411655
0.3	1.09453921	1.07970267	1.7710148	1.76741415
0.4	1.12227104	1.10731410	1.7914838	1.78776390
0.5	1.14534255	1.12919763	1.8096495	1.80617125

Continued on next page

Table 9 continued

E1	SWCNT	MWCNT	SWCNT	MWCNT
0.0	0.8837367	0.87895566	1.6811416	1.67751344
0.2	1.1024795	1.08686166	1.7383636	1.73459986
0.3	1.1504187	1.13312086	1.7599330	1.75616572
0.4	1.1839737	1.16566653	1.7795624	1.77581075
0.5	1.2065971	1.18771558	1.7981092	1.79443530
Fi	SWCNT	MWCNT	SWCNT	MWCNT
0.0	1.25465663	1.2353866	1.8912477	1.88789578
0.2	1.23600030	1.21764751	1.8872482	1.88400100
0.3	1.22689189	1.20898303	1.8853453	1.88214952
0.4	1.21792324	1.20044912	1.8835023	1.88035721
0.5	1.20908960	1.19204140	1.8817159	1.87862090
Po	SWCNT	MWCNT	SWCNT	MWCNT
0.1	1.25384014	1.23587080	1.8920906	1.88908341
0.2	1.23589200	1.21817013	1.8877372	1.88465776
0.3	1.21792324	1.20044912	1.8835023	1.88035721
0.4	1.19992910	1.18269312	1.8793809	1.87618108
0.5	1.18191964	1.16492279	1.8753815	1.87213790
ϕ	SWCNT	MWCNT	SWCNT	MWCNT
0.1	1.451888367	1.43652160	1.9150944	1.91381368
0.2	1.807616662	1.82721072	1.9471442	1.95227920
0.3	2.074458380	2.14474563	1.9642875	1.97435416
0.4	2.290496077	2.40732995	1.9787338	1.99106822
0.5	2.486432966	2.62236855	1.9954937	2.00759103

4 Conclusion

A numerical spatial simulation of the Darcy -Forchheimer flow explored with SWCNT and MWCNT on stretching in the presence of Joule heating, hall current with ion slip, and activation energy are carried out. The flow generating equations are converted into a system of coupled nonlinear ODEs and are solved numerically with python coding. The interesting conclusions of the present work are presented as follows:

- Electric field parameter has an important enhancing influence on velocity, temperature, and opposite nature on concentration. Investigators observed that the intermolecular force of CNT is the cause to reduce the concentration and increase the velocity and temperature.
- Velocity, concentration enhances and temperature decreases with increasing porosity. Researchers exploit the fact that absorption is the major cause of nanofluid explored with CNT.
- Investigators determined that temperature and concentration are positively correlated to inertial resistance, Velocity and inertial resistance are negatively correlated due to friction of CNT in a nanofluid.
- Investigators noticed that due to thermal conductivity and specific heat of Water, water-based carbon nanotube (SWCNT and MWCNT) profiles are enhanced when compared to the remaining base fluids except at concentration profile, because of the thermophoretic parameter of CNT.

This investigation is limited to study the deformation of nanofluids with carbon nanotubes with different base fluids using boundary value problems through python coding. Nowadays python code plays an important role to solve the nonlinear coupled ordinary differential equations to estimate the deformation of nanofluids even in the case of hybrid carbon nanotubes also.

5 Conflict of Interest

Investigators confirm that there is no conflict of interest to declare for this publication.

Nomenclature

B_0	Constant magnetic field intensity	m	Power of the exponential stretching sheet.
c_f	Inertial resistance	M_1	Electric parameter
c_p	Specific heat.	N	Fitted rate coefficient
C_w	Wall concentration	n_e	Hall current parameter
C_∞	Concentration outside the boundary layer	n_i	Ion-slip
D_B	Brownian diffusion coefficient.	N_b	Brownian motion parameter
D_T	Thermal diffusion coefficient.	N_t	Thermophoresis parameter
E	Activation energy parameter	P	Velocity components in x direction
E_0	Constant electric field intensity	P_r	Reference parameter
E_1	Electric parameter	P_o	Porosity parameter
E^*	Activation energy	P_r	Prandtl number
F_i	Inertial resistance parameter	Q	Velocity components in y direction
K	Boltzman constant	r	Velocity components in z direction
k_r	Reaction rate parameter.	R	Radiation parameter
K_{bf}	Thermal conductivity of basefluid	S_c	Schmidt number
K_{CNT}	Thermal conductivity of CNT	T_w	Wall temperature
K_{nf}	Thermal conductivity of nanofluid	T_∞	Temperature of the fluid outside the boundary layer
K^*	Permeability of porous media	x, y, z	Cartesian coordinates
L	Reference length.	β	Ratio of stretching rates parameter
Le	Lewies number	ε	Rotation parameter
me	Hall parameter	γ_C	Concentration Biot numbers
γ_T	Thermal Biot numbers	η	Similarity variable
δ_1	Temperature difference parameter	σ_{nf}	Electrical conductivity of nanofluid
δ_2	Reaction rate parameter	σ_{bf}	Electrical conductivity of basefluid
ρ_{bf}	Density of basefluid	σ_{CNT}	Electrical conductivity of CNT
ρ_{CNT}	Density of CNT	μ_{nf}	Coefficient of viscosity of nanofluid
ϕ	Nanoparticle volume fraction	μ_{bf}	Coefficient of viscosity of basefluid
θ	Dimensionless fluid temperature	ν_{nf}	Coefficient of kinematics viscosity of nanofluid

References

- Hayat T, Shafiq A, Alsaedi A. Effect of Joule Heating and Thermal Radiation in Flow of Third Grade Fluid over Radiative Surface. *PLoS ONE*. 2014;9(1):e83153. Available from: <https://dx.doi.org/10.1371/journal.pone.0083153>.
- Hayat T, Muhammad T, Shehzad SA, Alsaedi A. Similarity solution to three dimensional boundary layer flow of second grade nanofluid past a stretching surface with thermal radiation and heat source/sink. *AIP Advances*. 2015;5(1). Available from: <https://dx.doi.org/10.1063/1.4905780>.
- Sreenivasulu P, Reddy NB, and. Lie Group Analysis for Boundary Layer Flow of Nanofluids near the Stagnation-Point over a Permeable Stretching Surface Embedded in a Porous Medium in the Presence of Radiation and Heat Generation/Absorption. *Journal of Applied Fluid Mechanics*. 2015;8(3):549–558. Available from: <https://dx.doi.org/10.18869/acadpub.jafm.67.222.19373>.
- Khan U, Ahmed N, Mohyud-Din ST. Influence of viscous dissipation and Joule heating on MHD bio-convection flow over a porous wedge in the presence of nanoparticles and gyrotactic microorganisms. *SpringerPlus*. 2016;5(1). Available from: <https://dx.doi.org/10.1186/s40064-016-3718-8>.
- Afshar H, Shams M, Naeinian MM, Ahmadi G. Effect of Dispersed Nanoparticles on Thermophysical Properties of Nanofluid and Heat Transfer Coefficients. *Journal of Applied Fluid Mechanics*. 2016;9:165–171. Available from: [10.36884/jafm.9.SI1.25817](https://dx.doi.org/10.36884/jafm.9.SI1.25817).
- Sreenivasulu P, Poornima T, Reddy NB. Influence of Joule Heating and Non-Linear Radiation on MHD 3D Dissipating Flow of Casson Nanofluid past a Non-Linear Stretching Sheet. *Nonlinear Engineering*. 2019;8(1):661–672. Available from: <https://dx.doi.org/10.1515/nleng-2017-0143>.
- Shahzad F, Sagheer M, Hussain S. Numerical simulation of magnetohydrodynamic Jeffrey nanofluid flow and heat transfer over a stretching sheet considering Joule heating and viscous dissipation. *AIP Advances*. 2018;8(6). Available from: <https://dx.doi.org/10.1063/1.5031447>.
- Reddy JVR, Sugunamma V, Sandeep N. Simultaneous impacts of Joule heating and variable heat source/sink on MHD 3D flow of Carreau-nanoliquids with temperature dependent viscosity. *Nonlinear Engineering*. 2019;8(1):356–367. Available from: <https://dx.doi.org/10.1515/nleng-2017-0132>.
- Gholinia M, Gholinia S, Hosseinzadeh K, Ganji DD. Investigation on ethylene glycol Nano fluid flow over a vertical permeable circular cylinder under effect of magnetic field. *Results in Physics*. 2018;9:1525–1533. Available from: <https://dx.doi.org/10.1016/j.rinp.2018.04.070>.
- Singh J, Gupta M, Kumar R, Kumar H. Heat Transfer using Nanofluid. *International Journal of Engineering and Advanced Technology (IJEAT)*. 2019;9(2):3205–3211. Available from: [10.35940/ijeat.B9230.129219](https://dx.doi.org/10.35940/ijeat.B9230.129219).
- Srinivasacharya D, Jagadeeshwar P. Effect of Joule heating on the flow over an exponentially stretching sheet with convective thermal condition. *Mathematical Sciences*. 2019;13(3):201–211. Available from: <https://dx.doi.org/10.1007/s40096-019-0290-8>.

- 12) Tlili I, Nabwey HA, Ashwinkumar GP, Sandeep N. 3-D magnetohydrodynamic AA7072-AA7075/methanol hybrid nanofluid flow above an uneven thickness surface with slip effect. *Scientific Reports*. 2020;10(1). Available from: <https://dx.doi.org/10.1038/s41598-020-61215-8>.
- 13) Alzahrani A. Importance of Darcy-Forchheimer porous medium in 3D convective flow of carbon nanotubes. *Physics Letters A*. 2018;382(40):2938–2943. Available from: <https://doi.org/10.1016/j.physleta.2018.06.030>.
- 14) Majeed A, Zeeshan A, Noori FM. Numerical study of Darcy-Forchheimer model with activation energy subject to chemically reactive species and momentum slip of order two. *AIP Advances*. 2019;9(4). Available from: <https://dx.doi.org/10.1063/1.5095546>.
- 15) Muhammad T, Alsaedi A, Hayat T, Shehzad SA. A revised model for Darcy-Forchheimer three-dimensional flow of nanofluid subject to convective boundary condition. *Results in Physics*. 2017;7:2791–2797. Available from: <https://dx.doi.org/10.1016/j.rinp.2017.07.052>.
- 16) Ganesh NV, Hakeem AKA, Ganga B. Darcy-Forchheimer flow of hydromagnetic nanofluid over a stretching/shrinking sheet in a thermally stratified porous medium with second order slip, viscous and Ohmic dissipations effects. *Ain Shams Engineering Journal*. 2018;9(4):939–951. Available from: <https://dx.doi.org/10.1016/j.asej.2016.04.019>.
- 17) Hosseinzadeh K, Roghani SO, Mogharrebi AR, Asadi A, Waqas M, Ganji DD. Investigation of cross-fluid flow containing motile gyrotactic microorganisms and nanoparticles over a three-dimensional cylinder. *Alexandria Engineering Journal*. 2020;59(5):3297–3307. Available from: <https://dx.doi.org/10.1016/j.aej.2020.04.037>.
- 18) Hosseinzadeh K, Mardani MR, Salehi S, Paikar M, Waqas M, Ganji DD. Entropy generation of three-dimensional Bödewadt flow of water and hexanol base fluid suspended by Fe₃O₄ and MoS₂ hybrid nanoparticles. *Journal of Physics*. 2021;95(57). Available from: <https://dx.doi.org/10.1007/s12043-020-02075-9>.